Fractal dimension of transport coefficients in a deterministic dynamical system

2004 J. Phys. A: Math. Gen. 37 10859

(http://iopscience.iop.org/0305-4470/37/45/009)

INSTITUTE OF PHYSICS PUBLISHING JOURNAL OF PHYSICS A: MATHEMATICAL AND GENERAL

J. Phys. A: Math. Gen. **37** (2004) 10859–10877 PII: S0305-4470(04)78428-0

Fractal dimension of transport coefficients in a deterministic dynamical system

Zbigniew Koza

Institute of Theoretical Physics, University of Wrocław, pl. Maxa Borna 9, 50204 Wrocław, Poland

E-mail: zkoza@ift.uni.wroc.pl

Received 26 March 2004
Published 28 October 2004
Online at stacks.iop.org/JPhysA/37/10859
doi:10.1088/0305-4470/37/45/009

Abstract

In many low-dimensional dynamical systems, transport coefficients are very irregular and are perhaps even fractal functions of control parameters. To analyse this phenomenon, we study a dynamical system defined by a piecewise linear map and investigate the dependence of transport coefficients on the slope of the map. We present analytical arguments, supported by numerical calculations, showing that both the Minkowski–Bouligand and Hausdorff fractal dimension of the graphs of these functions is 1 with a logarithmic correction, and we find that the exponent γ controlling this correction is bounded from above by 1 or 2, depending on some detailed properties of the system. Using numerical techniques, we show local self-similarity of the graphs. The local self-similarity scaling transformations turn out to be dependent (irregularly) on the values of the system control parameters.

PACS numbers: 05.45.Df, 05.45.Ac, 05.60.Cd

1. Introduction

Various transport coefficients associated with a particle moving in a low-dimensional periodic array of scatterers are often very irregular functions of control parameters. For example, the diffusion coefficient of a particle moving in the flower-shaped billiard (a two-dimensional (2D) Lorentz gas with periodically distributed scatterers of six-petal flower shape) was found to be a very irregular function of the petal curvature [1], and the conductivity of the classical Lorentz gas (with disc scatterers) varies rapidly with the applied field [2]. The reaction rate and the diffusion coefficient in the reaction–diffusion multibaker model also turned out to be irregular, fractal-like functions of the map's shift [3]. Similar behaviour was found for the diffusion coefficient of a particle thrown onto a periodically corrugated floor and subject to various types of external force, including Hamiltonian [4] and dissipative [5, 6] systems. In chaotic systems with two degrees of freedom, the modes governing the relaxation to the

thermodynamic equilibrium form a fractal structure with a nontrivial fractal dimension that can be related to the Lyapunov exponent and the diffusion coefficient of the system [7–9]. Another example is provided by a deterministic dynamical system with dynamics defined by the iteration of a 1D map: the mean velocity and the drift coefficient in this system were shown to be irregular, nowhere differentiable functions of the system control parameters [10–14].

It is natural to ask what the origin of these 'irregularities' is, how to describe them quantitatively and to what extent they are universal. Answering all these questions is far from trivial. One of the reasons why the irregular behaviour of transport coefficients is so difficult to investigate is that, until very recently, our knowledge of this phenomenon was based mainly on numerical simulations. Although several different techniques for calculating these quantities were developed, e.g. the transition matrix technique combined with the escape-rate formalism [6, 13–18], the Green–Kubo formula [6, 14, 15] or the periodic-orbit formalism [15, 19], they all involve complicated and time-consuming numerical calculations of limited accuracy. Moreover, quite often, these techniques are applicable only for some special values of the control parameters. What is worse, as a model becomes more realistic, the results get less accurate. For this reason, the most precise data have been obtained for very simple, 1D 'toy models', while the question whether a more realistic 2D Lorentz gas (with scatterers of disc shape) exhibits any irregularity in the transport coefficient as a function of the disc radius is still a subject of controversy [6, 20].

This situation improved considerably when Groeneveld and Klages [10] gave exact formulae for the transport coefficients in a simple 1D deterministic dynamical system, introduced by Grossmann and Fujisaka [21] and defined by a piecewise linear map with two control parameters: the slope and the bias. Their solution has two important features. Firstly, it is complete, i.e. applicable for any (physically meaningful) value of the control parameters. Secondly, it reduces the problem of determining the transport coefficients to finding the sum of a quickly converging series. For the first time, we thus have a model exhibiting irregular behaviour of the transport coefficients, for which a solution permitting an efficient numerical implementation is available.

Klages and Klauß [11] have recently used this exact solution to examine in detail the irregular dependence of the drift velocity and diffusion coefficient on the control parameters of the system. Their aim was to verify an earlier hypothesis [12, 13] that the graphs of these quantities as functions of the map slope are so irregular that actually they form fractals. Using two numerical techniques: the box counting method and the autocorrelation function method, they found that the local fractal dimensions of these graphs are well defined on small finite subintervals, but are highly irregular functions of the control parameters. In other words, they found that these graphs cannot be described with a single fractal dimension, but rather with a set of quickly varying local fractal dimensions. Taking this into account, they put forward a hypothesis that the local fractal dimensions of these graphs as functions of the slope are themselves fractal.

However, our recent numerical calculations [22] suggest that the Minkowski–Bouligand fractal dimension Δ of the graph of the diffusion coefficient as a function of the slope is equal to 1 and that the convergence to this limit is slowed down by a logarithmic correction. Owing to this logarithmic term, the curve is a fractal. We also proposed a conjecture that the exponent controlling this correction depends on the slope of the map and equals either 1 or 2, depending on the existence and detailed properties of a Markov partition. That $\Delta = 1$ seems to be at odds with the above-cited results in [11], because the Minkowski–Bouligand dimension, if it exists, is equivalent to the box-counting dimension [23]. However, one should note that while we focused in our studies on the pointwise dimension calculated only for those system-control parameters that correspond to finite Markov partitions, Klages and Klauß computed

the box-counting dimension on intervals of finite length, and these two values need not be the same. The aim of our present study is to support our earlier findings analytically. We also present new numerical results that confirm these results.

The paper is organized as follows. Section 2 introduces the mathematical formalism. This includes the definition of the model, a brief description of the Minkowski–Bouligand dimension, the 'oscillation' method of calculating it for continuous curves and a precise formulation of our hypothesis about the logarithmic corrections. Our main results are contained in section 3, which presents a detailed calculation of the fractal dimension of the graph of the diffusion coefficient as a function of the slope for the case of zero bias. It also includes derivation of the upper bound for the exponent controlling the logarithmic corrections. Section 4 contains a brief discussion of how our results can be generalized for the case of arbitrary bias and for other transport coefficients. Section 5 contains numerical results. These include analysis of the factors determining the value of the logarithmic correction as well as a study of self-similarity of the graphs. Finally, section 6 is devoted to a discussion of the results and conclusions.

2. Basic formalism

2.1. The model

Following Groeneveld and Klages [10], we investigate a dynamical system with the equation of motion defined by a 1D map $M_{a,b} : \mathbf{R} \to \mathbf{R}$ parametrized by some real numbers a and b.

$$x_{n+1} = M_{a,b}(x_n), \tag{1}$$

where x_n represents the position of a particle and n is a discrete-time variable. The map is a piecewise linear function given by

$$M_{a,b}(x) = \begin{cases} ax + b, & x \in [-\frac{1}{2}, \frac{1}{2}), \\ M_{a,b}(x + n) - n, & x \in \mathbf{R}, \end{cases} \tag{2}$$

where n is an arbitrary integer, and the slope $a > 1$ and the bias $b \in \mathbf{R}$ are the control parameters of the system (detailed analysis of the system symmetries [10] leads to the conclusion that the values of b can be restricted to $-\frac{1}{2} \leqslant b < \frac{1}{2}$). The interval $[-\frac{1}{2}, \frac{1}{2})$ will be called 'the fundamental interval' and denoted by I_0^-. However, instead of I_0^-, one can choose $I_0^+ = (-\frac{1}{2}, \frac{1}{2}]$ as the fundamental interval in (2). It turns out that the transport coefficients (defined below) are the same whether we choose I_0^- or I_0^+ as the fundamental interval. This equivalence has been employed in the derivation of the explicit forms of the transport coefficients [10].

The main features of the dynamical system defined by map $M_{a,b}$ are depicted in figures 1(a) and 1(b). They show $M_{a,b}(x)$ for $a = 2.83$ and $b = 0.1$ and its action on two initial points x_0. In particular, figure 1(a) presents the trajectory of $x_0 = -\frac{1}{2}$ using the fundamental interval $[-\frac{1}{2}, \frac{1}{2})$, while figure 1($b$) shows the trajectory of $x_0 = \frac{1}{2}$ with the fundamental interval $(-\frac{1}{2}, \frac{1}{2}]$. We chose these two trajectories because, as will be explained, they determine all transport properties of the system. The trajectories seem to be rather weakly correlated (which is typical for $b \neq 0$) and 'random'. This randomness is related to the fact that, for nearly all values of a and b, the iteration of the deterministic map $M_{a,b}$ is equivalent to a stochastic Markov process of a random-walk type [17, 24, 25]: the deterministic trajectory of any point x_0 can be regarded as a particular realization of the random-walk process, and taking the average over the initial states x_0 is equivalent to taking the averages over the corresponding Gibbs ensemble. For this

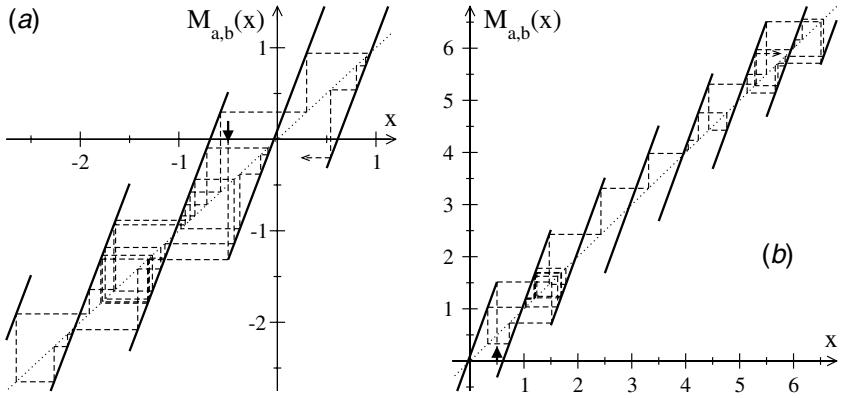

Figure 1. (*a*) The map $M_{a,b}(x)$ for particular values of the slope $a = 2.83$ and the bias $b = 0.1$ (thick solid lines); the dashed lines represent the first 33 terms of the trajectory of the point x_0 under subsequent iterations of M with $x_0 = -\frac{1}{2}$ and the fundamental interval I_0^-. The arrow indicates the initial position x_0. (*b*) The same as in (a), but for $x_0 = \frac{1}{2}$ and the fundamental interval I_0^+. In both cases, the transport coefficients are $J \approx 0.128$ and $D \approx 0.0543$.

reason, the process defined by $M_{a,b}$ (or similar maps) is often called 'deterministic diffusion'. The two basic transport coefficients, the drift velocity J and diffusion constant D, are defined as

$$J = \lim_{n\to\infty} \frac{\langle x_n \rangle}{n}, \qquad D = \lim_{n\to\infty} \frac{\langle x_n^2 \rangle - \langle x_n \rangle^2}{2n}, \tag{3}$$

where $\langle \cdots \rangle$ denotes the average over the uniform ensemble of initial values x_0. Figure 1 illustrates the effect of using different fundamental intervals. Had we generated both trajectories using the same fundamental interval, they would differ only by a simple translation defined by (2).

2.2. *Explicit form of the transport coefficients*

We will now briefly summarize Groeneveld and Klages' [10] method of calculating the transport coefficient for the model defined by the map $M_{a,b}$. For each $a > 1, b \in \mathbb{R}$, and $\epsilon = \pm$, one can define two infinite sequences of numbers, y_r^ϵ and n_r^ϵ, $r = 0, 1, \ldots$, consisting of reals and integers, respectively. Their values are uniquely determined by demanding that their first terms are given by

$$y_0^\epsilon = \frac{\epsilon}{2}, \qquad n_0^\epsilon = 0, \tag{4}$$

and for each $r > 0$,

$$n_r^\epsilon + y_r^\epsilon = a y_{r-1}^\epsilon + b, \tag{5}$$

with additional conditions

$$n_r^\epsilon \in \mathbb{Z} \qquad \text{and} \qquad y_r^\epsilon \in I_0^\epsilon. \tag{6}$$

Next, we define 'N-moments':

$$N_r^\epsilon = -\frac{\epsilon}{2} + \sum_{s=1}^{r} n_s^\epsilon, \tag{7}$$

$$N_{k,l}^\epsilon = \frac{1}{k!l!} \sum_{r=0}^{\infty} a^{-r} (N_r^\epsilon)^k r^l, \tag{8}$$

$$N_{k,l} = N_{k,l}^+ - N_{k,l}^-, \tag{9}$$

where $k, l \geqslant 0$. The basic transport coefficients, J and D, can now be expressed as ([10], cf [26])

$$J = \frac{N_{2,0}}{N_{1,1}}, \qquad D = \frac{N_{3,0} - N_{2,1} J + N_{1,2} J^2}{N_{1,1}}. \tag{10}$$

In the particular case of $b = 0$, we have, by symmetry, $J = 0$; hence the diffusion coefficient takes on a simpler form

$$D = \frac{N_{3,0}}{N_{1,1}}. \tag{11}$$

We will also use two important properties derived in [10]. Firstly,

$$N_{1,1} > 0, \tag{12}$$

so that D and J are well defined for any $a \neq 0$ and b. Secondly, all numbers n_r^ϵ are bounded:

$$|n_r^\epsilon| < \tfrac{1}{2} a + |b|. \tag{13}$$

2.3. Minkowski–Bouligand fractal dimension of the graph of a continuous function

Let E be a bounded set in the plane. The ϵ-Minkowski sausage of E, denoted by $E(\epsilon)$, is the set of all the points whose distance to E is less than ϵ. Let $\mathcal{A}(E(\epsilon))$ be the area of $E(\epsilon)$. Then, the Minkowski–Bouligand fractal dimension is defined as [23]

$$\Delta(E) = \lim_{\epsilon \to 0} \left(2 - \frac{\log \mathcal{A}(E(\epsilon))}{E(\epsilon)} \right), \tag{14}$$

provided that this limit exists. In this case, it is equivalent to the box-counting dimension [23]. A general relation between the Minkowski–Bouligand dimension Δ and the Hausdorff dimension Δ_H reads $\Delta \geqslant \Delta_H$. It is conjectured that, for all strictly self-similar fractals, $\Delta = \Delta_H$.

It has been recently proven [10] that the transport coefficients corresponding to the map $M_{a,b}$ are continuous (but not differentiable) functions of the slope a even though $N_{j,k}$ are generally not continuous in a. Therefore we can calculate Δ for the graphs of $D(a)$ or $J(a)$ using the fact that the Minkowski–Bouligand dimension of a continuous real function $f(t)$ defined on an interval $[t_0, t_1]$ can be evaluated through analysis of its Hölder exponents [23] and τ-oscillations [23]. The latter are defined as

$$\mathrm{osc}_\tau(f; t) = \sup_{|t-t'| \leqslant \tau} f(t') - \inf_{|t-t'| \leqslant \tau} f(t'). \tag{15}$$

The Hölder exponents are related to the oscillations as follows. If there exist constants $c > 0$ and $0 < H \leqslant 1$ such that, for all τ,

$$\mathrm{osc}_\tau(f; t) \leqslant c\tau^H, \tag{16}$$

then f is called a Holderian of exponent H at t. If constants c and H are independent of t, then the fractal dimension Δ of f satisfies

$$\Delta \leqslant 2 - H. \tag{17}$$

Similarly, if there exist constants $c > 0$ and H such that, for all τ,

$$\mathrm{osc}_\tau(f; t) \geqslant c\tau^H, \tag{18}$$

then f is called an anti-Holderian of exponent H at t; if c and H are independent of t, then

$$\Delta \geqslant 2 - H. \tag{19}$$

Relations (17) and (19) constitute a convenient means of calculating the Minkowski–Bouligand dimension Δ. Note that, although they are supposed to hold 'for all τ', in practice it suffices to prove their validity only in the limit of $\tau \to 0$.

2.4. Conjecture about the logarithmic correction to the fractal dimension

In [22], we proposed the following conjecture: for the map $M_{a,b}$ in the limit $\tau \to 0$,

$$\frac{\mathrm{osc}_\tau(D; a)}{\tau} \simeq \mathcal{C}(a)[-\log(\tau)]^{\gamma(a)}, \qquad \text{with} \quad \mathcal{C}(a), \gamma(a) > 0. \tag{20}$$

Together with (15)–(19), this implies that the fractal dimension of the graph of the diffusion coefficient D as a function of the control parameter a is equal to 1, but the convergence to this limiting value is logarithmically slow, with the exponent γ controlling the convergence rate.

To justify this statement, note that, since $\lim_{\tau\to 0}(-\log\tau)^\gamma/\tau^{H-1} = 0$ for any $\gamma \geqslant 0$ and $H < 1$, conjecture (20) implies that $D(a)$ is Holderian of any $H < 1$. Using (17), we find that the fractal dimension of its graph is bounded from above by any number of the form $2 - H$, with $H < 1$. Now we can take the limit of $H \uparrow 1$ to see that Δ cannot exceed 1. Similarly, (20) implies that $D(a)$ is anti-Holderian of exponent $H = 1$, and so $\Delta \geqslant 1$. Hence, $\Delta = 1$.

In the above analysis, we have tacitly assumed that the coefficient $\mathcal{C}(a)$ in (20) can be bounded from below and above by positive constants independent of a. We will address this problem in section 5.2.

Since D is a continuous, nowhere differentiable function of a [10], the fractal dimension Δ must be $\geqslant 1$ and exponent γ must be strictly positive. This reasoning constitutes an alternative derivation of the lower bound for Δ and explains why $\gamma(a) > 0$. Our numerical calculations (performed for the bias $b = 0$) indicated that exponent γ depends on the slope a and is equal to either 1 or 2, depending on periodicity properties of the sequences $y_k^\pm$ [22]. In particular, we conjectured that $\gamma = 2$ for the slopes a generating disjoint sequences y_k^+ and y_k^-, and $\gamma = 1$ otherwise.

Note that, even though $\Delta = 1$, the graph of $D(a)$ is not an ordinary, smooth curve of dimension 1. Actually, owing to the logarithmic term in (20), this graph is nowhere rectifiable (i.e. any of its arcs is 'of infinite length'), which is typical of fractals [23]. Therefore the graph of $D(a)$ locally resembles a well-known family of Takagi functions [6, 14, 15, 23], for their graphs are also nonrectifiable, their dimension is $\Delta = 1$, and they satisfy (20) with $\gamma(a) = 1$ for all a. Takagi functions appear naturally in many contexts related to deterministic diffusion [6, 7, 14, 15].

Since hypothesis (20) opens a convenient way to explore the fractal properties of graphs of the diffusion coefficient, its detailed analysis, carried out with both analytical and numerical methods, is one of the main goals of our present paper.

3. Fractal dimension of the diffusion coefficient for $b = 0$

In the case of zero bias ($b = 0$), the diffusion coefficient D vanishes for the slopes $a \leqslant 2$. Therefore we shall consider only the nontrivial case of

$$a > 2. \tag{21}$$

The basic properties of the diffusion coefficient are encoded in the sequences (n_k^{ϵ}), introduced in section 2.1. Before we are able to tackle the problem of evaluating the fractal dimension of $D(a)$, we need to derive several useful properties of these sequences.

3.1. Basic properties of n_k and y_k for $b = 0$

3.1.1. Symmetry. For $b = 0$, the sequences $n_k^{\pm}$ and $y_k^{\pm}$ satisfy

$$n_k^+ = -n_k^-, \qquad y_k^+ = -y_k^-, \tag{22}$$

so it will suffice to concentrate on the sequences n_k^+ and y_k^+; for simplicity, we will denote these terms as n_k and y_k, respectively. These sequences may be either periodic or not periodic. Periodic sequences n_k (and y_k) correspond to the so-called Markov partitions of the interval I_0^+ (or I_0^-) [13, 14, 17, 24]. The parameters a for which the sequences n_k and y_k are periodic will be called 'Markov slopes'. They form a dense set on $(1, \infty)$ [10].

3.1.2. Discontinuity in a. The numbers n_k, as well as y_k, can be considered as functions of a. Equation (5) implies that all functions $n_k(a)$ and $y_k(a)$, $k = 1, 2, \ldots$, are discontinuous in a, which has a profound impact on the functional dependence of the transport coefficients J and D on a. This is illustrated in figure 2. Figure 2(a) presents the quantity of our primary interest: the diffusion coefficient D as a function of the slope a for $4 \leqslant a \leqslant 6$ and for the vanishing bias $b = 0$. Although highly irregular, this function is continuous [10]. One might expect that so are $N_{3,0}(a)$ and $N_{1,1}(a)$, because their quotient is equal to D. However, as depicted in figures 2(b) and (c), they are actually discontinuous. From (7)–(9), we conclude that this must be related to discontinuity of functions $n_k^{\pm}(a)$. Two of them, $n_2^+(a)$ and $n_3^+(a)$, are shown in figures 2(d) and (e), respectively (as horizontal line segments). For completeness, in the same figures are also depicted the graphs of $y_2^+(a)$ and $y_3^+(a)$. As expected, there is a clear correlation between discontinuities of $n_k(a)$, $y_k(a)$ and discontinuities of $N_{3,0}(a)$, $N_{1,1}(a)$. Moreover, there is also a correlation between these discontinuities and 'irregularities' of $D(a)$.

The union of all the discontinuity points of $n_k(a)$ for all k will be denoted by Ξ and we will introduce $\bar{\Xi}$ as the complement of Ξ on the interval $(1, \infty)$. The importance of these two sets is related to the fact that functions $N_{k,l}(a)$ are continuous on $\bar{\Xi}$ and discontinuous on Ξ. Moreover, functions $n_k(a)$ and $y_k(a)$ are also continuous on $\bar{\Xi}$ (however, in contrast to $N_{k,l}(a)$, they can also be continuous on some points of Ξ). Both Ξ and $\bar{\Xi}$ are dense on $(1, \infty)$ [10].

3.1.3. Approximate linearity of $y_k(a)$. Figures 2(d) and (e) suggest that $y_2(a)$ and $y_3(a)$ consist of almost linear segments even though, in reality, they are polynomials of degrees 2 and 3, respectively. Moreover, the density of discontinuity points of n_3 is considerably greater than that of n_2. These two important observations can be justified in a more formal way. First of all, note that (5) implies

$$y_k' = y_{k-1} + a y_{k-1}' = \sum_{j=0}^{k-1} y_{k-1-j} a^j, \tag{23}$$

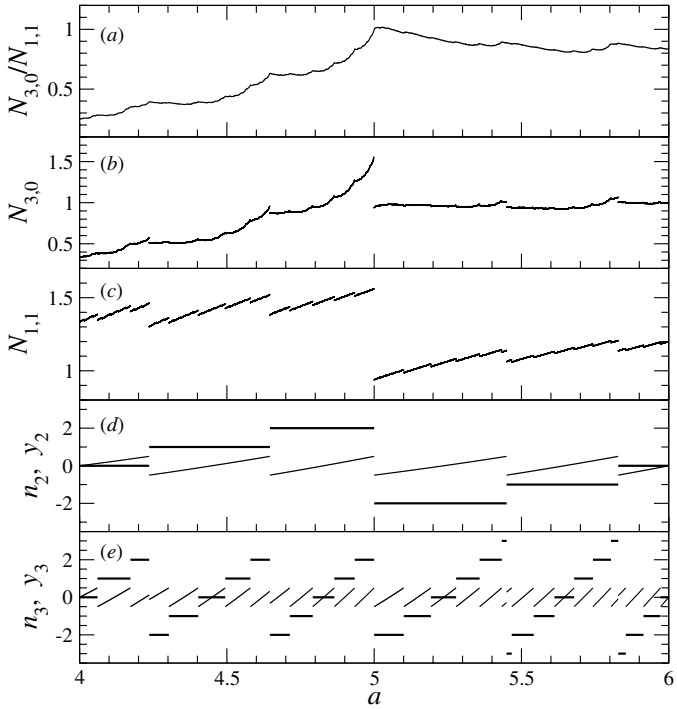

Figure 2. Graphs of the basic quantities used in the mathematical derivation as functions of the slope a, calculated for the bias $b = 0$. (*a*) The diffusion coefficient $D = N_{3,0}/N_{1,1}$, (*b*) N_{30}, (*c*) N_{11}, (*d*) n_2 (horizontal, thick lines) and y_2 (thinner curves) and (*e*) n_3 (horizontal, thick lines) and y_3 (thinner, almost linear curves). Except for D, all of them are discontinuous. N_{jk} are continuous on a dense set $\bar{\Xi}$ and discontinuous on a dense set Ξ, which is the union of all the discontinuity points of $n_1(a)$, $n_2(a)$, $n_3(a)\ldots$ (see text for details).

where we used a short-hand notation $y_k' = \mathrm{d}y_k(a)/\mathrm{d}a$. Therefore, since $|y_k(a)| \leqslant \frac{1}{2}$ and $y_0 = \frac{1}{2}$, the derivative $\mathrm{d}y_k(a)/\mathrm{d}a$ is bounded

$$\frac{a^{k-1}(a-2)+1}{2(a-1)} \leqslant y_k' \leqslant \frac{a^k-1}{2(a-1)}. \tag{24}$$

Taking into account (21), we conclude that, for large k,

$$y_k' \sim a^{k-1}. \tag{25}$$

Since the range of each y_k is limited to $[-\frac{1}{2}, \frac{1}{2}]$, the distance between two consecutive discontinuity points of $y_k(a)$, denoted as $\delta_k(a)$, is of order $\lesssim a^{1-k}$, i.e. decreases rapidly with k. Similar reasoning leads to the conclusion that the second derivative of $y_k(a)$ is of order $\lesssim 2(k-1)a^{k-1}$. Thus the maximal error resulting from truncating the Taylor series of $y_k(a)$ after the linear term for the displacement $\delta_k(a) \sim a^{1-k}$ is of order $(k-1)/a^{k-1}$ and vanishes quickly as k goes to infinity. Therefore functions $y_k(a)$ can actually be approximated to high accuracy by piecewise linear segments.

3.1.4. The limits of a going to a_0 from below and from above. Although functions $N_{k,l}(a)$ are discontinuous on Ξ, they are left-continuous. Moreover, it turns out that, for any $a_0 \in (1, \infty)$, the limit of $N_{k,l}(a)$ for a going to a_0 from above is also well defined. We will denote it

by $\tilde{N}_{k,l}(a_0)$. Its value can be related to $N_{k,l}(a_0)$ as follows. For $a_0 \in \bar{\Xi}$, by definition of $\tilde{\Xi}$, $\tilde{N}_{k,l}(a_0) = N_{k,l}(a_0)$. On the other hand, for $a_0 \in \Xi$, the sequence $n_0(a_0), n_1(a_0), \ldots$ is strictly periodic. Denoting the period length by L, we thus have $n_k(a_0) = n_{k+L}(a_0)$ for all $k \geqslant 0$. For a tending to a_0 from above, the sequence $n_k(a)$ will converge to a new sequence, $\tilde{n}_k(a_0)$

$$\tilde{n}_k(a_0) = \begin{cases} n_k(a_0), & k < L, \\ n_k(a_0) + 1, & k = L, \\ -n_k(a_0), & k > L. \end{cases} \tag{26}$$

Now, $\tilde{N}_{k,l}(a_0) = \lim_{a \to a_0+} N_{k,l}(a_0)$ can be determined upon substituting $\tilde{n}_k(a_0)$ for n_k in (7)–(9). Functions $\tilde{N}_{k,l}(a)$ are right-continuous. As argued in [10], all transport coefficients of the system defined by the map $M_{a,b}$ are continuous in a. Consequently, functions $\tilde{N}_{k,l}(a_0)$ can replace $N_{k,l}(a)$ in (10) to calculate the transport coefficients of the system. It is also interesting to note that, even though the functions $N_{k,l}(a)$ and $\tilde{N}_{k,l}(a)$ are different, their graphs must be the same. For this reason, figure 2(*b*) actually shows both $N_{3,0}(a)$ and $\tilde{N}_{3,0}(a)$. A similar conclusion pertains also to figure 2(*c*).

3.2. Oscillations at elements of $\bar{\Xi}$

Let a_0 be an arbitrary element of $\bar{\Xi}$. This means that all functions $y_k(a)$ are continuous at a_0, and so for each integer k, there exists $\varepsilon_0 > 0$ such that $y_0, y_1, \ldots, y_k$ and $n_0, n_1, \ldots, n_k$ are continuous and differentiable functions of a on the interval $(a_0 - \varepsilon_0, a_0 + \varepsilon_0)$. Therefore, for any $a \in (a_0 - \varepsilon_0, a_0 + \varepsilon_0)$, all functions $n_j(a)$ up to $j = k$ are independent of a. Let $0 < \tau < \varepsilon_0$. Since $y_k(a)$ is continuous on $(a_0 - \varepsilon_0, a_0 + \varepsilon_0)$, we can write down its Taylor expansion about a_0 and, following our discussion in section 3.1.3, truncate it after the linear term, obtaining $y_k(a_0 + \tau) \approx y_k(a_0) + \tau y_k'(a_0)$.

Let $\mu(\tau; a)$ be the maximum integer j such that $y_j(a)$ and $n_j(a)$ are continuous on $(a - \tau, a + \tau)$. This means that, for any $a_0 \in \bar{\Xi}$ and a fixed μ, numbers μ and τ are related through $y_\mu(a_0) + \tau y_\mu'(a_0) \approx \frac{1}{2}$ or $y_\mu(a_0) - \tau y_\mu'(a_0) \approx -\frac{1}{2}$ (whichever gives smaller τ). This, together with (25), leads to the following implicit equation for $\mu(\tau; a)$:

$$\mu(\tau; a) \approx \log_a \frac{\frac{1}{2} - |y_{\mu(\tau;a)}|}{\tau}. \tag{27}$$

There are two cases: the sequence $y_0(a_0), y_1(a_0), \ldots$ is either periodic (i.e. the system has a Markov partition) or not. In the former case, the numerator in (27) is bounded from above and below by *positive* numbers; in the limit $\tau \to 0$, we thus have

$$\mu(\tau; a) \approx \log_a \tau^{-1} + \text{const} \qquad \text{for } a \in \bar{\Xi}. \tag{28}$$

Clearly, $\mu(\tau; a) \to \infty$ as $\tau \to 0$. In other words, in the limit $\tau \to 0$ (which is essential for the analysis of Hölder exponents), the number of functions in the sequences $y_k(a)$ and $n_k(a)$ that are continuous on $(a - \tau, a + \tau)$ goes to infinity.

The case where the sequence $y_0(a_0), y_1(a_0), \ldots$ is not periodic is far more complicated. The main problem comes from the fact that now the numerator in (27) can get arbitrarily close to zero, which may invalidate (28). In the present approach, we restrict ourselves to the cases where the system has a Markov partition and so the sequence $y_0(a_0), y_1(a_0), \ldots$ is periodic.

As expressed by (11), the diffusion coefficient is the quotient of two quantities, $N_{3,0}$ and $N_{1,1}$. However, by a straightforward calculation, we can verify that, for any $\tau > 0$ and any functions $f(t)$ and $g(t)$ bounded on $[t - \tau, t + \tau]$ (no matter if continuous or not, but the lower

bound for $|g|$ must be $\neq 0$),

$$\operatorname{osc}_\tau(f/g) = \max_\tau(f/g) - \min_\tau(f/g) \leqslant \frac{\operatorname{osc}_\tau(f)\max_\tau(g) + \operatorname{osc}_\tau(g)\min_\tau(f)}{\min_\tau(g)\max_\tau(g)}$$

$$\leqslant c_1 \operatorname{osc}_\tau(f) + c_2 \operatorname{osc}_\tau(g), \tag{29}$$

where we used a short-hand notation $\max_\tau(f) \equiv \sup_{|t-t'|\leqslant\tau} f(t')$ and $\min_\tau(f) \equiv \inf_{|t-t'|\leqslant\tau} f(t')$, while c_1 and c_2 are some nonnegative parameters independent of τ.

Owing to (12), we can apply (29) to $D(a)$, substituting $N_{3,0}$ for f, $N_{1,1}$ for g and a for t. The problem of finding the τ-oscillations of the diffusion coefficient D can be thus reduced to that of finding $\operatorname{osc}_\tau(N_{3,0}; a)$ and $\operatorname{osc}_\tau(N_{1,1}; a)$.

Equation (8) implies that, for arbitrary integers k, l and $a = a_0 \pm \tau$,

$$N_{k,l}(a_0) - N_{k,l}(a) \leqslant \frac{2}{k!l!} \sum_{r=\mu(\tau;a_0)}^{\infty} \{a_0^{-r}[N_r^+(a_0)]^k - a^{-r}[N_r^+(a)]^k\} r^l, \tag{30}$$

with μ related to τ through equation (28). Here we have employed the fact that, by the definition of μ, $n_r(a) = n_r(a_0)$, and hence $N_r^+(a) = N_r^+(a_0)$ for all $r < \mu(\tau; a)$. Using (13), we conclude that

$$|N_r^+| \leqslant c_1^* r + c_2^*, \tag{31}$$

with $c_1^* \geqslant 0$, $c_2^* > 0$ being some constants. It will be convenient to assume that c_1^* denotes the smallest possible value satisfying (31), $c_1^* \equiv \limsup_{r\to\infty} |N_r^+(a_0)|/r$.

Owing to (31), an upper (as well as lower) bound for $N_{k,l}(a_0) - N_{k,l}(a)$ can be found by substituting arithmetic sequences for $N_r^+(a_0)$ and $N_r^+(a)$ in (30). Their common differences may be different, but the terms for $r = \mu$ must be the same or differ by a small number less than $\frac{1}{2}a + |b|$ (cf (13)). This leads to

$$|N_{k,l}(a) - N_{k,l}(a_0)| \lesssim a^{-\mu}\mu^{k+l-1} \qquad \text{for } c_1^* > 0, \tag{32}$$

$$|N_{k,l}(a) - N_{k,l}(a_0)| \lesssim a^{-\mu}\mu^{l} \qquad \text{for } c_1^* = 0. \tag{33}$$

This important result can also be obtained by noticing that the major contribution to the sum in (30) comes from its first few terms. Hence, using (28),

$$|N_{k,l}(a_0 \pm \tau) - N_{k,l}(a_0)| \lesssim \tau \ln^{k+l-1}(\tau^{-1}), \qquad c_1^* > 0, \tag{34}$$

$$|N_{k,l}(a_0 \pm \tau) - N_{k,l}(a_0)| \lesssim \tau \ln^{l}(\tau^{-1}), \qquad c_1^* = 0, \tag{35}$$

which implies

$$\operatorname{osc}_\tau(N_{k,l}; a) \lesssim \tau \ln^{k+l-1}(\tau^{-1}), \qquad c_1^* > 0, \tag{36}$$

$$\operatorname{osc}_\tau(N_{k,l}; a) \lesssim \tau \ln^{l}(\tau^{-1}), \qquad c_1^* = 0. \tag{37}$$

Consequently, by (29) and (11),

$$\operatorname{osc}_\tau(D; a) \lesssim \tau \ln^{2}(\tau^{-1}), \qquad c_1^* > 0, \tag{38}$$

$$\operatorname{osc}_\tau(D; a) \lesssim \tau \ln(\tau^{-1}), \qquad c_1^* = 0 \tag{39}$$

for all $a \in \bar{\Xi}$.

Equations (38) and (39) give the upper bound for the exponent γ controlling the logarithmic correction to the local fractal dimension. As we can see, this upper bound depends on c_1^*. This constant has a simple physical interpretation. If the trajectories of points $x_0 = \pm\frac{1}{2}$ under $M_{a,b}$ (like those depicted in figure 1) remain confined inside a neighbourhood of the origin, we can take $c_1^* = 0$, which implies $0 < \gamma \leqslant 1$. Otherwise $c_1^* > 0$ and $0 < \gamma \leqslant 2$.

3.3. Oscillations at elements of Ξ

The argumentation presented in section 3.2 might seem of little use for elements of the set Ξ, at which functions $N_{k,l}(a)$ are discontinuous. However, functions $N_{k,l}(a)$ are left-continuous and have a well-defined limit from the right, $\tilde{N}_{k,l}(a)$. Functions $\tilde{N}_{k,l}(a)$ are right-continuous and, as argued in section 3.1.3, can replace $N_{k,l}(a)$ in calculations of the transport coefficients. This suggests a method of circumventing the problems related to discontinuity. The oscillation of the diffusion coefficient D on the interval $[a_0 - \tau, a_0 + \tau]$ with $a_0 \in \Xi$ can be calculated as the maximum of two values: the oscillation of $(N_{3,0}/N_{1,1})(a)$ on $[a - \tau, a]$ and the oscillation of $(\tilde{N}_{3,0}/\tilde{N}_{1,1})(a)$ on $[a, a + \tau]$. In each case, we can now apply the reasoning of section 3.2 (its most delicate point, validity of approximation (28), can be justified rigorously because the sequence $n_k(a)$ is periodic for all $a \in \Xi$). This implies that (38) and (39) are valid also for all $a \in \Xi$, which suggests that the fractal dimension of the diffusion coefficient is 1 for all Markov slopes $a \in (1, \infty)$.

4. The case $b \neq 0$

Besides the fractal properties of the diffusion coefficient D, in the asymmetric case $b \neq 0$ we can also investigate those of the drift J, which for $b \neq 0$ is also a highly irregular function of the control parameters [10]. It turns out that the methods developed in section 3 can be readily extended to the case of nonvanishing bias b and to the analysis of arbitrary transport coefficients. Therefore we will only discuss the major differences and difficulties that appear when applying these methods to the more general case $b \neq 0$.

Firstly, although derivation of the basic relation (27) remains practically unchanged, we see that restricting our calculations to the case $1 < a \leqslant 2$ is fully acceptable only for $b = 0$. This is related to the fact that, for $b \neq 0$, the transport coefficients can assume nontrivial values also for $a \leqslant 2$ [10], so this parameter region also deserves attention. The assumption $a > 2$ greatly simplifies the proof of (25) (cf (24)); without it, we have to take into account correlations between consecutive terms of the sequences $y_k^{\pm}$. Our numerical analysis shows that (24), and hence (27), is valid also for $1 < a \leqslant 2$ (at least in the limit $k \to \infty$), but we failed to find a rigorous proof of it.

Secondly, the sequences n_k^+ and n_k^- are no longer related to each other by (22) and, in practice, must be considered as independent of each other. This, fortunately, is not a serious difficulty—actually relation (22) was used mainly to simplify notation.

Thirdly, just as in the case $b = 0$, we can justify transition from (27) to (28) only in the case where both n_k^+ and n_k^- are periodic, i.e. when the system has a Markov partition.

Finally, we still need an analytical argument justifying our claim that the graph of $(D; a)$ is *uniformly* anti-Holderian for all b.

Although, in section 3, we focused on the fractal properties of the diffusion coefficient D, our analysis was as general as possible. In particular, inequalities (36) and (37) were derived for functions $N_{k,l}(a)$ with arbitrary k, l. Since all transport coefficients, including the drift velocity J, can be expressed as functions of the quotients $N_{k,l}/N_{1,1}$ [10], the methods of section 3 can be applied for arbitrary transport coefficients.

Consequently, we can follow the ideas of section 3 to argue that the local fractal dimension of the graphs of transport coefficients as functions of a is equal to 1 for the control parameters a and $b \in \mathbf{R}$ such that $a > 2$ and the system has a Markov partition. Based on our numerical calculations [22] and heuristic arguments, we conjecture the same fractal behaviour for all other pairs (a, b).

5. Numerical results

5.1. The role of c_1^*

Equations (38) and (39) imply that the exponent γ controlling the logarithmic correction is bounded from above by 2 for $c_1^* > 0$ and by 1 for $c_1^* = 0$. On the other hand, however, in [22], we conjectured that the value of γ depends on properties of the periods of sequences y_k^+ and y_k^- (i.e. whether they consist of the same or different terms). A question arises whether the two approaches lead to the same conclusions for γ and, if not, what does its value really depend on?

To answer it, we will study a particular case of the bias $b = 0$ and the slope a equal to the largest root of $a^5 - 2a^4 - 2a^3 + 2a^2 + 1$, i.e. $a \approx 2.455$. The trajectory of $x_0^+ = \frac{1}{2}$ is $x_1^+ \approx 1.23, x_2^+ \approx 1.56, x_3^+ \approx 0.92, x_4^+ \approx 0.80, x_5^+ = x_0^+, \ldots$, and so the sequence x_m^+ is periodic, $x_{5+m}^+ = x_m^+$. The trajectory of x_0^- is given by $x_m^- = -x_m^+$, and hence is periodic, too. Since all the terms of the sequence x_k^- are different from those of x_k^+, the value of γ should be 2 according to [22]. This is in conflict with (39), as the trajectories of $x_0 = \pm\frac{1}{2}$ are bounded, hence $c_1^* = 0$ and, following (39), $\gamma \leqslant 1$. We checked this numerically using the arbitrary precision arithmetic library GMP (http://www.swox.com/gmp). Our results are presented in figure 3. They clearly suggest that $\gamma = 1$. This implies that our earlier hypothesis about the logarithmic correction exponent γ was incorrect. Our present, deeper insight into the mathematical nuances of the problem leads to the conclusion that the main factor determining the value of γ (at least for systems with periodic trajectories of $x_0 = \pm\frac{1}{2}$) is whether the constant c_1^* vanishes or not.

Figure 3, especially the inset, indicates also that, in the case of the map $M_{a,b}$, oscillations of the diffusion coefficient really deserve their name. Apparently, the graph of $\mathrm{osc}_\tau(D)/\tau$ as a function of $\log \tau^{-1}$ is composed of a linear and a periodic 'oscillating' function. The period length λ of these 'oscillations of oscillations' can be estimated using (28),

$$\lambda = a^L, \tag{40}$$

where L is the period of $y_k^\pm$; in our case, $L = 5$, $\lambda = a^5 \approx 89$ and $\log \lambda \approx 1.95$, in excellent agreement with the data in figure 3.

5.2. Uniformly Hölder and anti-Hölder conditions for $D(a)$

As we explained in section 2.4, analysis of Hölder exponents can be useful in the exploration of fractal properties of a curve if this curve is uniformly Holderian (or anti-Holderian), i.e. if the coefficient $\mathcal{C}(a)$ in (20) can be bounded from below (or above) by a constant number. We decided to check these properties numerically for the vanishing bias b, as in this particular case, all Markov slopes a are algebraic numbers. They can thus be generated in a systematic way by first generating polynomials with integer coefficients and then identifying Markov slopes with the largest roots of the polynomials. Moreover, the coefficients of each such polynomial determine the numbers n_r^ϵ, hence determine whether the constant c_1^* vanishes or not, and thus whether the exponent $\gamma(a)$ in our conjecture (20) is expected to equal 1 or 2, respectively.

To check whether $D(a)$ is uniformly anti-Holderian, we concentrated on the case $\gamma(a) = 1$, i.e. $c_1^* = 0$. Using a computer program, we found *all* Markov slopes $a \in (2; 8]$ that are algebraic numbers of degree $d \leqslant 4$ and correspond to $c_1^* = 0$. Then, for each such slope, we calculated the coefficient $\mathcal{C}(a)$. To this end, we assumed that, at each investigated slope, the graph of $\mathrm{osc}_\tau(D; a)$ as a function of $\log \tau^{-1}$ behaves like the one depicted in figure 3. To increase

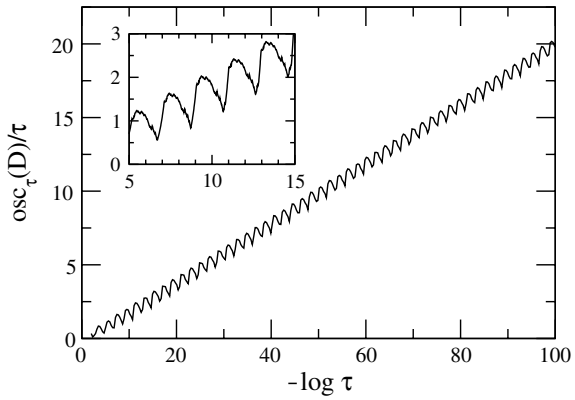

Figure 3. Oscillations of the diffusion coefficient D for $b = 0$ and a equal to the largest root of $a^5 - 2a^4 - 2a^3 + 2a^2 + 1$, i.e. $a \approx 2.455$, rescaled in accordance with (20) and calculated on intervals $(a - \tau, a + \tau)$ for $10^{-100} \leqslant \tau \leqslant 10^{-2}$. The inset presents an enlarged view of the results and reflects the periodicity of the curve.

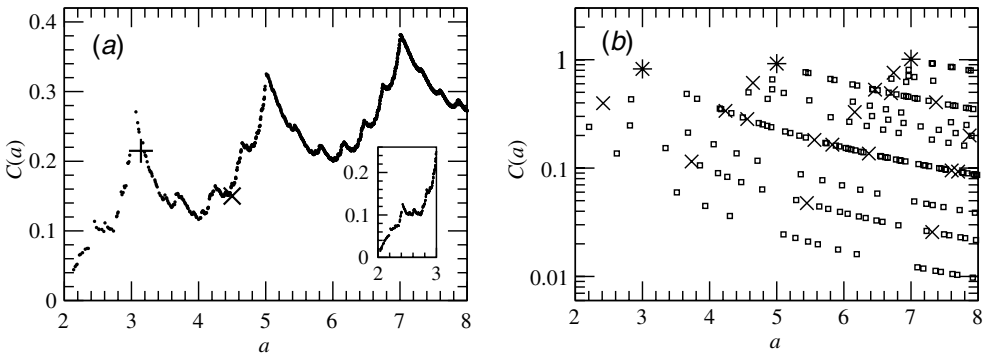

Figure 4. (*a*) The coefficient $\mathcal{C}(a)$ for all Markov slopes $a \in (2; 8]$ that correspond to $\gamma = 1$ and are algebraic numbers of degree $d \leqslant 4$ (2054 data points). The inset presents the same quantity calculated for $a \in (2; 3]$ and $d \leqslant 6$ (439 data points). The plus (+) and cross (×) signs mark the estimated values of $\mathcal{C}(a)$ for non-Markov slopes $a = \pi$ and $a = 4.5$, respectively. (*b*) Same as in (*a*), but for $\gamma = 2$ and $d = 1$ (asterisks), $d = 2$ (crosses) and $d = 3$ (open squares). The logarithmic scale for the ordinate axis was used to visualize the structure of $\mathcal{C}(a)$.

accuracy, we eliminated local periodic oscillations of the curves by using (40). As expected, the points of each curve at abscissas forming an arithmetic sequence with a common difference $\log \lambda$ turned out to form practically a straight line with the slope quickly converging; we identified this limiting slope with $\mathcal{C}(a)$. In each case, the sum of squares of the residuals from the best-fit line was less than 10^{-10}. The results obtained in this way are depicted in figure 4(*a*). As expected, the density of the points increases with a. Moreover, apparently they lie on a *continuous* curve that crosses the x-axis only at $a = 2$. These findings are supported by the results depicted in the inset of this figure and obtained for all Markov slopes $a \in (2; 3]$ that correspond to $c_1^* = 0$ and $d \leqslant 6$. That $\mathcal{C}(a)$ tends to a continuous curve implies that the graph of D as a function of a is uniformly anti-Holderian with $H = 1$ and $\gamma = 1$ at least on the set of all Markov slopes $a > 2$ for which $c_1^* = 0$. Note that this set is dense on $(2, \infty)$.

To check whether $D(a)$ is uniformly Holderian, we focused on the Markov slopes with $\gamma(a) = 2$, i.e. $c_1^* \neq 0$. We investigated numerically all Markov slopes $a \in (2; 8]$ that are algebraic numbers of degree $d \leqslant 3$ and correspond to $c_1^* \neq 0$ (286 data points). We found that, at each such slope, the exponent γ is actually equal to 2. However, as seen in figure 4(b), the coefficient $\mathcal{C}(a)$ turned out to be a highly irregular, discontinuous function of a. Fortunately, this function is apparently bounded from above. Taking into account our earlier result for $c_1^* = 0$, we conclude that the graph of the diffusion coefficient D as a function of the slope a is uniformly Holderian (with $H = 1$ and $\gamma = 2$) at least on the (dense) set of all Markov slopes.

Analysis of the Hölder and anti-Hölder conditions at non-Markov slopes is far more difficult. Such values of a were already investigated numerically in [22]. The conclusion was that, in this case, most probably $\gamma = 1$, but this property cannot be definitely established numerically due to very poor convergence. In several cases, there is a clear linear trend in graphs of $\mathrm{osc}_\tau(D; a)$ as a function of $\log \tau^{-1}$, which permits us to estimate the value of $\mathcal{C}(a)$ (assuming $\gamma(a) = 1$). For example, using the data of [22], we can estimate that $\mathcal{C}(\pi) \approx 0.215$ and $\mathcal{C}(4.5) \approx 0.15$. As seen in figure 4, these values are very close to those obtained for the nearby Markov slopes. However, for many other values of a, no reasonable numerical estimation of $\mathcal{C}(a)$ is possible.

5.3. Oscillations of $N_{k,l}(a)$

Results of section 3.2 reveal that the logarithmic corrections to fractal dimensions of graphs of transport coefficients can be attributed to similar logarithmic corrections in functions $N_{k,l}(a)$. For $a \in \tilde{\Xi}$, these latter functions are continuous in a and we expect them to satisfy (20) with $N_{k,l}$ substituted for D, i.e. for $\tau \to 0$,

$$\frac{\mathrm{osc}_\tau(N_{k,l}; a)}{\tau} \sim [\log(\tau^{-1})]^{\gamma_{k,l}(a)}, \tag{41}$$

where, following (36) and (37),

$$0 \leqslant \gamma_{k,l} \leqslant k + l - 1 \qquad \text{for } c_1^* > 0, \tag{42}$$

$$0 \leqslant \gamma_{k,l} \leqslant l \qquad \text{for } c_1^* = 0. \tag{43}$$

This conjecture relates the fractal nature of transport coefficients to fractality of the functions $N_{k,l}(a)$, which—although of no immediate physical meaning—have a much simpler form and are more amenable to rigorous treatment.

To verify (41)–(43), we have calculated oscillations of $N_{3,0}$ and $N_{1,1}$ for the vanishing bias b and two values of the slope a: the largest root of $a^5 - 4a^4 + 2a^3 + 3a^2 - 2a + 4$ (i.e. for $a \approx 3.04$) and the largest root of $a^5 - 4a^4 - 4a^2 + a + 4$ (i.e. for $a \approx 4.20$). For these parameter values, the system has a Markov partition [22]; moreover, the constant $c_1^* = 0$ for $a \approx 3.04$ and $c_1^* > 0$ for $a \approx 4.20$.

Our results for $a \approx 3.04$ and $a \approx 4.20$ are depicted in figures 5(a) and (b), respectively. As we can see, our data clearly indicate that, in both cases, $\gamma_{1,1} = 1$. However, $\gamma_{3,0} = 0$ in figure 5(a) (i.e. for $c_1^* = 0$) and $\gamma_{3,0} = 2$ in figure 5(b) (i.e. for $c_1^* > 0$). All these results are in perfect agreement with (43) and actually correspond to the upper bounds implied by these equations. Note that, for $c_1^* = 0$, equation (43) actually gives not only the upper bound, but the exact value of $\gamma_{k,0} = 0$ for all $k > 0$.

The insets to figure 5 suggest that, just as in the case of graphs of $\mathrm{osc}_\tau(D)/\tau$ discussed in section 5.1, on finer scales the graphs of $\mathrm{osc}_\tau(N_{k,l})/\tau$ as functions of $\log \tau^{-1}$ have periodic components. Their period lengths λ can be calculated using (28), which gives $\lambda = a^6 \approx 794$

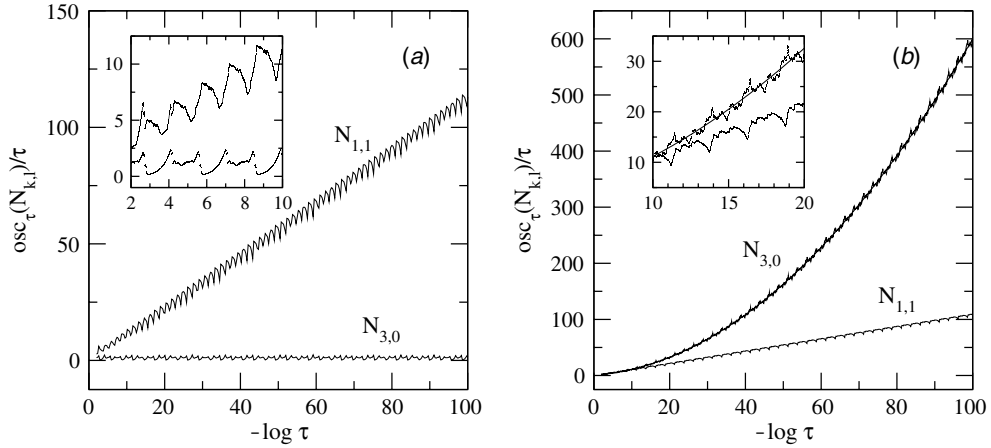

Figure 5. Oscillations of $N_{1,1}$ and $N_{3,0}$, rescaled in accordance with (41) and calculated on intervals $(a-\tau, a+\tau)$ for $10^{-100} \leqslant \tau \leqslant 10^{-2}$, with $b = 0$ and a equal to the largest root of (*a*) $a^5 - 4a^4 + 2a^3 + 3a^2 - 2a + 4$ and (*b*) $a^5 - 4a^4 - 4a^2 + a + 4$. Results for $N_{3,0}$ in (*b*) were fitted by a quadratic (a solid line, hardly distinguishable from numerical data). The insets are blowups of the curves to show their periodicity and discontinuity in a.

for $a \approx 3.04$ (figure 5(*a*)) and $\lambda = a^4 \approx 311$ for $a \approx 4.20$ (figure 5(*b*)). These theoretical values are in excellent agreement with the numerical data used to produce figure 5.

5.4. Self-similarity of the graphs

In the limit $\tau \to 0$, the periodicity of the curves presented in figures 3 and 5 becomes practically perfect. This phenomenon could be a consequence of local self-similarity of functions $D(a)$ and $N_{k,l}(a)$ under enlargement of their graphs by a scale factor λ. To verify this hypothesis, in figure 6(*a*) we have plotted the graph of the diffusion coefficient D as a function of the slope a, with the origin moved to the point $a_0 \approx 2.455$ and $D_0 \equiv D(a_0) \approx 0.0967$. Then, we plotted three consecutive blowups of this graph, obtained by magnifying it about the new origin by scale factors λ, λ^2 and λ^3, where $\lambda = a_0^5 \approx 89$. As seen in figure 6(*a*), this simple transformation of graphs does not lead to perfectly self-similar structures; nevertheless, the curves thus obtained do exhibit some kind of similarity.

The effect of actual self-similarity can be achieved if each λ-fold enlargement is followed by a correction transformation related to the nonvanishing logarithmic correction exponent γ. The two-step transformation T can be expressed as

$$T(x, y) = (\lambda x, \lambda y - \kappa_1(\lambda x)), \tag{44}$$

where λ is the scale factor and κ_1 is a correction term. Our numerical results suggest that, for $\gamma = 1$, this complementary step is a simple linear transformation, $\kappa_1(x) = sx$, with s being a constant depending on the slope a, the bias b and the function the self-similarity transformation T is applied to. In the case of the data shown in figure 6, the constant $s \approx -0.1969$. The net effect of this two-step scaling procedure applied iteratively $m = 0, 1, 2, 3$ times is depicted in figure 6(*b*). As we can see, the convergence is very fast and the curves obtained after $m = 1, 2$ and 3 elementary two-step transformations are already practically indistinguishable from each other. Closer analysis of the numerical data for $m = 0, \ldots, 10$ revealed that, with each two-step transformation, we get closer to the self-similar limit curve by about two significant figures. Similar behaviour was found for several other points a_0, both for graphs of the diffusion

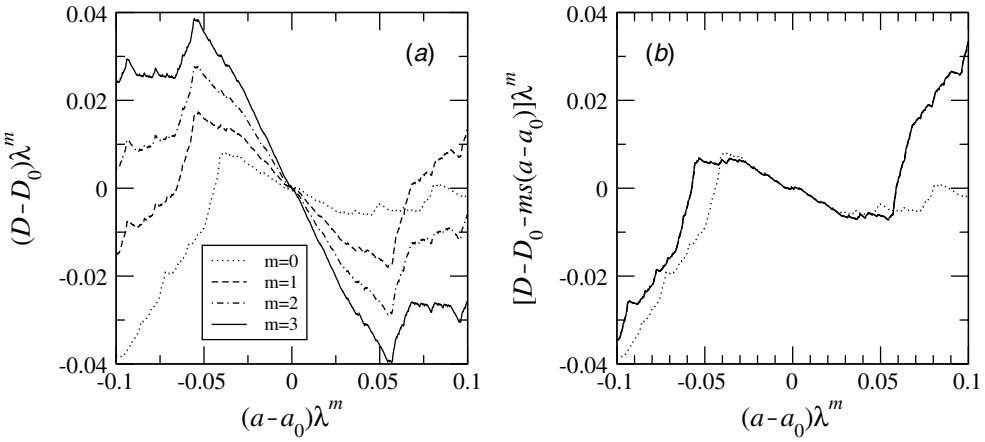

Figure 6. (*a*) A graph of the diffusion coefficient obtained for the slope $a_0 \approx 2.455$ and the bias $b = 0$ (dotted line) and its consecutive λ-fold magnifications about the point (a_0, D_0), where $\lambda = a_0^5 \approx 89$ and $D_0 \equiv D(a_0) \approx 0.0967$. (*b*) Same as in (*a*), except that now each λ-fold magnification has been followed by a linear transformation $(x, y) \mapsto (x, y - sx)$ with $s \approx -0.1969$; all four curves have been plotted, but those obtained for $m = 1, 2, 3$ differ from each other by less than the line width.

coefficient $D(a)$ and the auxiliary functions $N_{1,1}(a)$, $N_{3,0}(a)$, provided that the corresponding logarithmic correction exponent γ was 1. Note that transformation of type (44) holds also for Takagi functions.

For $\gamma = 1$, the net effect of applying consecutively m transformation T is

$$T_m(x, y) = (\lambda^m x, \lambda^m y - m\kappa_1(\lambda^m x)), \tag{45}$$

where linearity of the correction term in m corresponds to $\gamma = 1$. For $\gamma = 2$, the situation gets more complicated. We now expect that the correction term after m self-similarity transformations is quadratic in m,

$$T_m(x, y) = (\lambda^m x, \lambda^m y - m^2\kappa_2(\lambda^m x) - m\kappa_1(\lambda^m x)), \tag{46}$$

with some real functions κ_1 and κ_2. A side-effect of such a form of the correction term is that, in contrast to the case $\gamma = 1$, the second steps in each elementary two-step transformation now depend on m, and hence slightly differ from each other. We have confirmed (46) numerically, finding the convergence to be very fast. In particular, figure 7 presents the results obtained for the slope $a_0 \approx 4.20$ and bias $b_0 = 0$ (these parameters were already used in figure 5(*b*)). In the left panel, we show correction functions κ_1 and κ_2. As we can see, κ_2 is linear, while κ_1 is an irregular (perhaps fractal) function of its argument. Although the graph of $\kappa_1(x)$ in figure 7(*a*) is quite similar to that of $D(a)$ (dotted line in figure 7(*b*)), these two functions are different. In the right panel, we present the effects of applying T_m, $m = 0, 1, 2, 3$, to the graph of $D(a)$ in the vicinity of the point $(a_0, D(a_0))$. Convergence to the self-similar limit is very fast. Actually, for $m > 1$, the graphs of T_m in figure 7(*b*) differ from each other by less than the line width.

6. Summary and conclusions

We have analysed both analytically and numerically the local (Minkowski–Bouligand) fractal dimension of graphs of transport coefficients as functions of the slope a in a simple dynamical

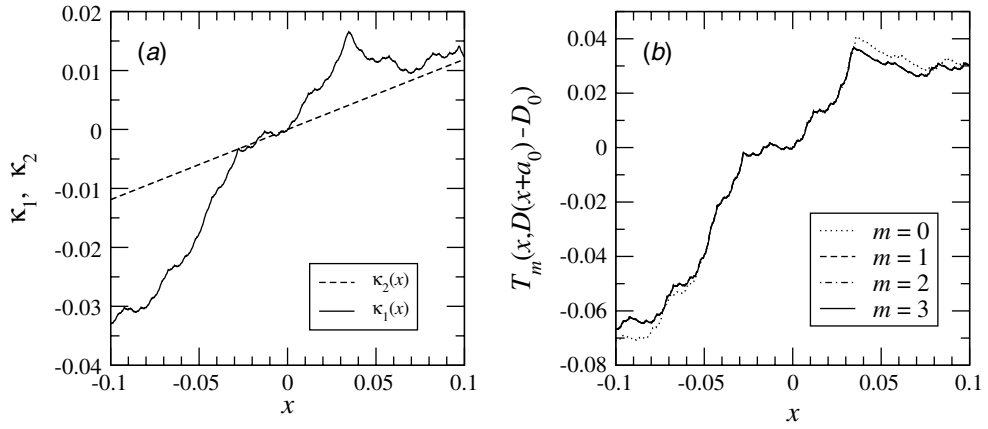

Figure 7. (a) Correction functions κ_1 and κ_2 used in the self-similarity transformation (46) for the graph of the diffusion coefficient $D(a)$ about the point (a_0, D_0) with $a_0 \approx 4.20$, $D_0 = D(a_0)$ and the bias $b = 0$. (b) The self-similarity effect of applying T_m, as described by (46), to the graph of $D(a)$, for the same parameter values as those used to generate (a). Note that the dotted line (corresponding to $m = 0$) actually represents the graph of the original function $D(a)$ translated by a vector $(-a_0, -D_0)$ and x can be interpreted as $\lambda^m(a - a_0)$. The graphs obtained for $m \geqslant 1$ are practically indistinguishable from each other.

system defined by a piecewise linear map $M_{a,b}$. We showed that, for all values of the control parameters a and b such that the system defined by $M_{a,b}$ has a Markov partition, the dimension of such graphs is 1, probably with a logarithmic correction. This correction renders the curves nowhere rectifiable (i.e. any of their arcs is 'of infinite length'), which is typical of fractals. Our results imply also that the Hausdorff dimension of these curves is 1.

We have also found the upper bound for the exponent γ controlling the logarithmic correction. This bound turned out to be either 1 or 2, depending on whether a constant c_1^* vanishes or not or, equivalently, whether the trajectories of $x_0 = \pm\frac{1}{2}$ remain bounded or not. This finding extends our earlier conjecture [22] about factors determining the value of γ.

Using numerical calculations, we have shown that, at Markov slopes a, the graph of the diffusion coefficient is actually self-similar under the action of a special, two-step scaling transformation. The first step is a simple uniform enlargement by a scale factor λ. This transformation must be followed by the second step, a 'correction' transformation of the graph, which is related to the nonzero value of the exponent γ controlling the logarithmic correction to the local fractal dimension. We found the precise formula for the value of the scale factor λ as well as a general form of the correction transformations. In particular, we found that the scale factor λ depends on the slope a and the periodicity of the trajectories of points $x_0 = \pm\frac{1}{2}$. The correction transformations turned out to be linear (affine) for $\gamma = 1$ and different, more complicated for $\gamma = 2$. At non-Markov slopes, the graphs are probably not self-similar.

The graphs of transport coefficients have thus a surprisingly rich spectrum of local fractal properties. Our numerical results suggest that the curves are self-similar on a dense set of points (at which the system has a Markov partition), but at each such point the scale factor and the correction transformation are different. In this sense, the curves are multifractals.

Our analytical approach has, however, some limitations. The most serious one is related to the fact that it is applicable only to systems in which the trajectories of points $x_0 = \pm\frac{1}{2}$ are periodic (or, equivalently, to systems with a Markov partition). We believe that the typical value of γ at non-Markovian slopes a is 1, but in general this value can take on any value between 1

and 2. This conjecture, however, requires further studies. Proving that the investigated curves are *uniformly* Holderian with $H = 1$ and $\gamma = 2$ and anti-Holderian with $H = 1$ and $\gamma = 1$ is another open problem. So far, we have been able to justify these properties only numerically.

Numerical results suggest that our analytical approach gives not only the upper bound, but the exact value of γ. To prove this hypothesis rigorously would require finding a 'tight' lower bound for γ. However, as is well known [23], finding the lower bound of a fractal dimension is usually much more difficult than finding the upper one. This is also true in our case. For example, when we were looking for the upper bound of oscillations of the quotient of two functions, we did not have to take into account the fact that actually their values were correlated. Applying the same general assumption for the lower bound of γ yields only a trivial result $\gamma \geqslant 0$. Therefore finding a better lower bound for the logarithmic correction is another problem for future studies.

Another question is how to reconcile our results with those obtained by Klages and Klauß [11], who analysed the box-counting dimension of $D(a)$ on intervals of *finite* length and found it to be greater than 1. One possible way of answering this problem could be to analyse how the local self-similarity of the curves depends on the box size.

Although most of our analysis was carried out explicitly for the graph of the diffusion coefficient D as a function of the slope a for a vanishing bias b, we showed how it can be generalized for other transport coefficients and for arbitrary bias b. Similarly, we expect that the main conclusions derived here for the simple piecewise linear map $M_{a,b}$ remain valid also in the case of more realistic (and complex) dynamical systems. After all, in our model, the main reason for irregular, fractal dependence of the transport coefficients on the slope a is an extreme sensitivity of the (periodic) Markov orbits on the control parameters; a similar sensitivity is observed in more complex models, e.g. the multibaker or the Lorentz gas [1–3, 6, 17]. Transport coefficients in these models were already called 'fractal', but only in the sense of 'unexpectedly irregular'. We hope that our present approach will help justify a conjecture that the transport coefficients in those more realistic models form fractals in a strictly mathematical sense of the term.

Acknowledgments

I thank R Klages for introducing me to the subject, many invaluable remarks on the paper and inspiration to write section 5.2. Support from the Polish KBN grant no 2 P03B 030 23 is also gratefully acknowledged.

Note added in proof. Another dynamical system with a highly irregular dependency of transport coefficients on control parameters was recently studied in [27].

References

[1] Harayama T, Klages R and Gaspard P 2002 *Phys. Rev.* E **66** 026211
[2] Lloyd J *et al* 1995 *Chaos* **5** 536
[3] Gaspard P and Klages R 1998 *Chaos* **8** 409
[4] Harayama T and Gaspard P 2001 *Phys Rev.* E **64** 036215
[5] Mátyás L and Klages R 2004 *Physica* D **187** 165
[6] Klages R 2003 Microscopic chaos, fractals, and transport in nonequilibrium steady states *Habilitation Thesis* Max Planck Institut, Dresden
[7] Gilbert T, Dorfman J R and Gaspard P 2001 *Nonlinearity* **14** 339
[8] Gaspard P, Claus I, Gilbert T and Dorfman J R 2001 *Phys. Rev. Lett.* **86** 1506
[9] Claus I and Gaspard P 2002 *Physica* D **168** 266

[10] Groeneveld J and Klages R 2002 *J. Stat. Phys.* **109** 821
[11] Klages R and Klauß T 2003 *J. Phys. A: Math. Gen.* **36** 5747
[12] Klages R and Dorfman J R 1995 *Phys. Rev. Lett.* **74** 387
[13] Klages R and Dorfman J R 1999 *Phys. Rev.* E **59** 5361
[14] Klages R 1996 *Deterministic Diffusion in One-Dimensional Chaotic Dynamical Systems* (Berlin: Wissenschaft und Technik Verlag)
[15] Dorfman J R 1999 *An Introduction to Chaos in Nonequilibrium Statistical Mechanics* (Cambridge: Cambridge University Press)
[16] Gaspard P and Nicolis G 1990 *Phys. Rev. Lett.* **65** 1693
[17] Vollmer J 2002 *Phys. Rep.* **372** 131
[18] Gaspard P 1992 *J. Stat. Phys.* **68** 673
[19] Cvitanović P *et al* 2003 *Chaos: Classical and Quantum* (Copenhagen: Niels Bohr Institute), http://www.nbi.dk/ChaosBook/
[20] Klages R and Dellago Ch 2000 *J. Stat. Phys.* **101** 145
[21] Grossmann S and Fujisaka H 1982 *Phys. Rev.* A **26** 1779
[22] Koza Z 2004 *Acta Phys. Polon.* B **35** 1365
[23] Tricot C 1995 *Curves and Fractal Dimension* (Berlin: Springer)
[24] Nicolis G and Nicolis C 1988 *Phys. Rev.* A **38** 427
[25] Claes I and Van den Broeck C 1993 *J. Stat. Phys.* **70** 1215
[26] Koza Z 1999 *J. Phys. A: Math. Gen.* **32** 7637
[27] Gilbert T and Dorfman J R 2004 *Disc. Cont. Dyn. Sys.* B **4** 391